Experimental Analysis of the Thermal Unbalance Effect of a Flexible Rotor Supported by a Flexure Pivot Tilting Pad Bearing

Thibaud PLANTEGENET, Mihai ARGHIR, Pascal JOLLY

Institut Pprime, UPR CNRS 3346, Université de Poitiers, ENSMA, Chasseneuil du Poitou, France.

Abstract

The Morton effect is a thermally induced increase of synchronous vibrations amplitudes of rotors. The shearing of the fluid film in a journal bearing produces an asymmetric heating of the rotor which causes its thermal bending and increases the unbalance. The vector of synchronous vibrations describes a spiral with slowly increasing amplitude and phase change. The thermal bending is also enlightened by a hysteresis effect of the synchronous vibrations during start-up and coast-down. The purpose of this study is to highlight experimentally the signature of Morton effect in a flexible rotor supported by a flexure pivot tilting pad journal bearing. A dedicated test rig has been built. It consists of a flexible rotor guided at one end by a ball bearing and at the other end by a flexure pivot tilting pad bearing. The tests consist of controlled start-ups to a speed close to the critical speed of the first rotor flexible mode, followed by controlled coast-downs. They show a hysteresis of the amplitudes and phases of the synchronous vibrations. Other tests performed at constant speeds show amplitude and phase variations corresponding to spiral vibrations. The results are explained by the non-uniform distribution of the rotor temperature.

Keywords: **Morton effect, experimental analysis, flexible rotor, tilting pad bearing.**

1 Introduction

Instabilities of thermally induced synchronous vibrations in rotors are not always well understood because they are a combination of thermal and rotordynamic effects. Three sources of heat generation can be distinguished in rotordynamics. The first is the thermal induced vibration instability caused by a light contact between the rotor and a seal. This is known as the Newkirk effect. It was discovered in 1926 [1] and was well studied in the 70s, being now well understood ([2]-[5]). The second is the Morton effect where the source of heat generation is the lubricant shearing in a hydrodynamic bearing. This effect was first studied by Morton [6] in 1975 and by Hesseborn [7] in 1978, but has received particular attention only since the 1990s. Three reviews were recently published ([8], [9] and [10]), showing that

the Morton effect is still a problem in rotordynamics. The third effect is caused by the electromagnetic iron loss in active magnetic bearings but just few studies exists on this subject [11], [12].

1.1 Physical description of the thermally induced unbalance effect

The Newkirk effect is the easiest to explain and helps understanding on how a heat source may generate unstable synchronous vibrations. The present description is inspired from reference [5] (pp. 306-313). A light rub may occur between the rotor and a part of the stator (for example a seal) when a misalignment between shaft and stationary part is present or when the synchronous vibrations due to mechanical unbalance are large. Due to the synchronous nature of the vibrations, contact occurs always at the same point on the rotor. This point is called the high spot (because the radial clearance is minimal) and will characterize the vibration vector. The heat generated by the Coulomb friction force will be maximum at the contact point. This point, characterised by the highest temperature, is called the hot spot (HS). For the Newkirk effect, the hot spot coincides with the high spot. The hot spot will induce a thermal bending of the rotor that can be viewed as an additional unbalance. Depending on the rotor-bearing system, the thermally induced unbalance can be in phase with the hot spot, or out of phase. Two simple but representative rotor-bearing systems are presented in **Figure 1**.

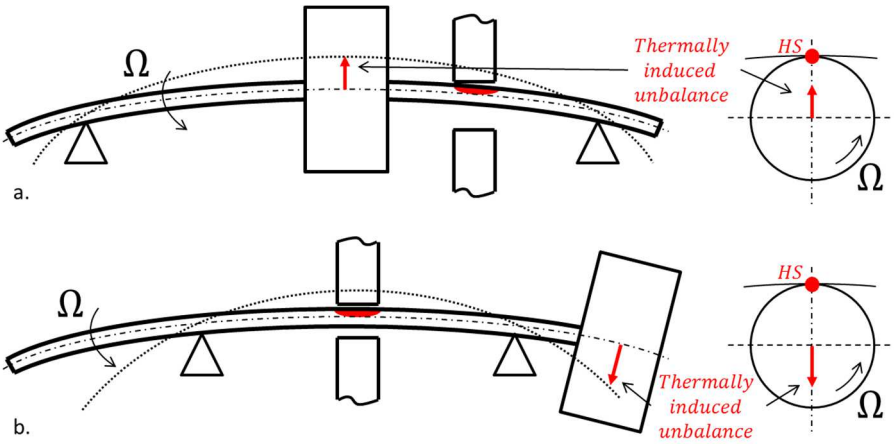

Figure 1. Thermally induced unbalance. a) in phase with the HS. b) out of phase with the HS.

In addition to the thermal unbalance, the mechanical unbalance is always present at the same point on the rotor called the heavy spot. The two unbalance vectors will be added to create a total unbalance. The phase difference between the synchronous vibration vector and the total unbalance vector depends on the operating conditions. If the rotational speed is less than the first critical speed then the phase

between the synchronous vibration vector and total unbalance vector is between 0° and 90° and if it is above the first critical speed, the phase is between 90° and 180°.

Four situations can be distinguished and are described in the ***Table 1***. The vectors $\overrightarrow{F_{th}}$, $\overrightarrow{F_u}$ are the thermal and the mechanical unbalance force, respectively; $\overrightarrow{F_{res}}$ is the resulting unbalance force (thermal and mechanical). The angle β is the phase between the mechanical unbalance (heavy spot) and the synchronous vibration vector (high spot). The angle ϕ describes the position of the vibration vector relative to the zero-phase reference (Key).

Table 1. Different situations induced by the thermal unbalance effect

Rotational speed	Thermally induced unbalance in phase with HS	Thermally induced unbalance out of phase with HS
Subcritical	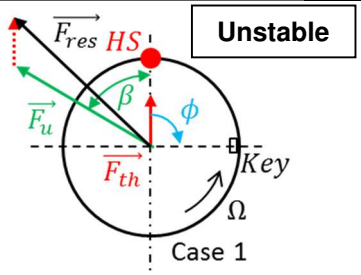	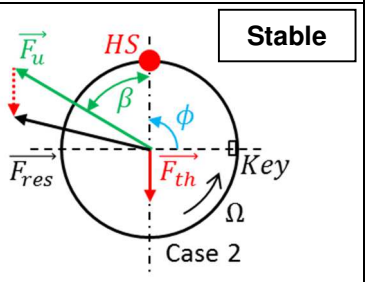
Supercritical	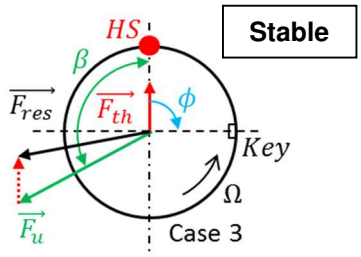	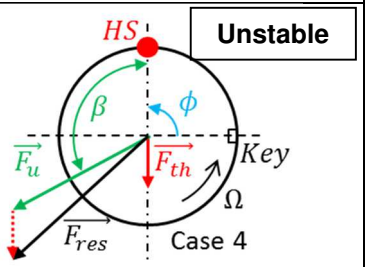

Case 1: the thermally induced unbalance is in phase with the hot spot and the rotational speed is subcritical. The thermal unbalance leads to the increase of the total unbalance. The vibration vector increases and rotates against the rotational speed (the phase angle ϕ varies as indicated in **Table 1**). The vibration vector describes a divergent spiral with increasing amplitude and continuously varying phase (**Figure 2**a.). This corresponds to an instability.

Case 2: the thermally induced unbalance is out of phase with the hot spot and the rotational speed is subcritical. The thermal unbalance leads to a decrease of the total unbalance. The vibration vector

decreases and rotates in the direction of the rotational speed. The vibration vector tends to an equilibrium position (**Figure 2**b.) and the rotor system is stable.

Case 3: the thermally induced unbalance is in phase with the hot spot and the rotational speed is supercritical. The thermal unbalance leads to a decrease of the total unbalance. The vibration vector decreases and rotates against the rotational speed. The vibration vector tends to an equilibrium position (**Figure 2**c.) and the rotor system is stable.

Case 4: the thermally induced unbalance is out of phase with the hot spot and the rotational speed is supercritical. The thermal unbalance leads to an increase of the total unbalance. The vibration vector increases and rotates in the direction of the rotational speed. The vibration vector describes a divergent spiral with increasing amplitude and continuously varying phase (**Figure 2**d.). The rotor system is unstable.

Furthermore, in some cases, the vibration vector is at the frontier between the cases 1-2 or 3-4 and describes a limit cycle with continuously varying phase and amplitude (cyclic vibrations).

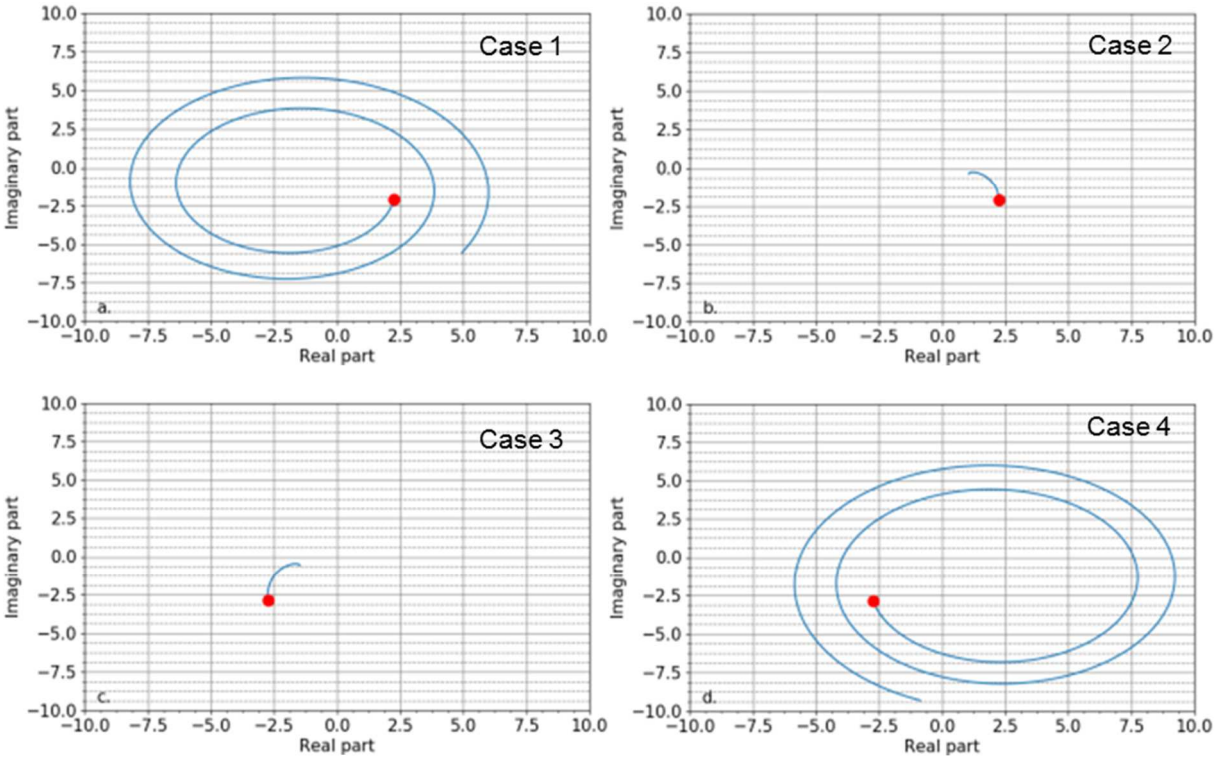

Figure 2. Trajectories of the vibration vector for situations modeled in Table 1 (the marker indicates the initial conditions)

This description of thermal induced synchronous vibration instabilities holds for the Newkirk effect but it is also useful for understanding the Morton effect. The main difference between these effects is the way

heat is generated. For the Morton effect, the shearing of the lubricant film in a journal bearing generates the heat and the rubbing contact is absent. Consequently, the hot spot considerably precedes the high spot. This is the main qualitative difference between the Newkirk and the Morton effect.

1.2 Industrial cases and previous experimental investigations of the Morton effect

In 1975, Morton [6] measured the temperature difference (ΔT), at the surface of a rotor supported by a journal bearing of 711 mm diameter and operating at 1800 rpm. He showed a linear relation between the ΔT and the amplitudes of synchronous vibrations. In 1978, Hesseborn [7] confirmed this linear relation.

In 1996, de Jongh and Morton [13] showed that a centrifugal compressor using lubricated bearings and designed to operate at 12 krpm, well below the second bending mode located at 14.5 krpm, presented synchronous spiral vibrations close to 11 krpm. The spiral vibration disappeared when the speed was lowered to 10 krpm and the amplitudes showed a hysteresis effect. The instability was still present after improving the rotor balancing and diminishing the overhung mass, but at 13.1 krpm. The overhung mass had to be lowered again for operating without spiral vibrations.

In 1998, de Jongh and van der Hoeven [14] presented a complex industrial case of two centrifugal compressors showing cycling synchronous vibrations when operated on site. Successive retrofits showed that the occurrence of the phenomena depended on the environmental temperature. They eliminated the problem by retrofitting the journal bearings with an isolating air chamber.

In 1999, Berot and Dourlens [15] analyzed a series of compressors similar to the one in [13]. The compressors had different overhung masses. Three of five compressors showed an unstable behavior close to the maximum continuous operating speed and the drive end bearing exhibited large amplitude, synchronous, centered vibration. The authors concluded that the unstable behavior was due to the non-uniform journal heating. They tried many solutions for curing the instability but only reducing the ratio of the length and the diameter of the bearing lead to a stable behavior because the orbits became elliptic and eccentric.

Kocur and de Jongh [16] presented another Morton effect for a centrifugal compressor with an overhung mass. When rapidly accelerated at constant speed the rotor showed an increase of the synchronous vibrations followed by a stabilization. The authors introduced a thermal barrier between the bearing and

the casing for reducing the amplitudes of synchronous vibrations. For other compressors the solution was simply the modification of the radial clearance and the decrease of the overhung mass.

In 2007, Marscher and Illis [17] presented a compressor operating on tilting pad bearings that generated cyclic synchronous vibrations after its oil feeding system was retrofitted. The problem was solved by increasing the oil feeding temperature.

Schmied et al. [18] published in 2008 the analysis of a turbo blower composed of a rotor with two overhung disks supported by two tilting pad bearings. The compressor showed spiral diverging synchronous vibrations when approaching the first critical speed. Stiffening the rotor improved the stability but did not cured it completely. The authors further reduced the length of the bearings and modified the viscosity of the lubricant.

In 2011, Lorenz and Murphy [19] analyzed four rotating machinery of identic design but showing different synchronous spiral vibrations: stable, unstable and cyclic. For remedying the instability, the partial arc bearings were replaced by lobe bearings.

The above-cited references described industrial cases and retrofitting solutions. Dedicated test rigs were built starting with the work of de Jongh and van der Hoeven [14] who confirmed experimentally that a journal bearing could generate a non-uniform heating of a rotor. The rotor was therefore instrumented with four temperature probes and a slip ring at its non-drive end.

Balabahadur [20] modified a test rig that consisted of a rotor supported by two tilting pad bearings and an overhung mass. The author showed a hysteretic behavior of synchronous vibrations but the presence of the Morton effect was not confirmed because the rotor temperatures were not measured.

In 2012, Bradley [21] developed a modular test rig that could operate with different kind of journal bearings and with a rigid or a flexible rotor. The Morton effect was not enlightened but the author observed that the increase of rotor temperature was associated to the increase of the unbalance and of the synchronous orbit amplitude.

Panara et al. [22] have also built a test rig to confront the theoretical predictions of Murphy and Lorenz [23] with their own model. The test rig consists of a rotor supported by two tilting pad bearings. A slip ring recorded the measured rotor temperatures and overhung disks of different masses enabled the test

of three rotor configurations. The authors showed that the instability of synchronous vibrations is related to the overhung mass.

In 2018, Tong and Palazzollo [24] presented a test rig developed for the validation of a numerical model of the Morton effect. The test rig consists of an eccentric rotor supported by two ball bearings and describing an imposed orbit. A tilting pad journal bearing is mounted between the ball bearings. The rotor is instrumented with temperature probes. The measurements showed that the phase lag between the hot and the high spot was comprised between 20°@1.2 krpm and 40°@5.5krpm. Moreover, Hresko and Palazzollo [25] presented in 2019 a test rig under development for the experimental simulation of the Morton effect.

The present work is the continuation of experimental investigations for simulating the Morton effect in a simple rotor presented in [26]. The test rig consists of a hollow rotor supported by a ball bearing at its drive end and by a journal bearing at its non-drive end. A flexure pivot tilting pad bearing replaces the simple cylindrical journal bearing used in [26]. This kind of journal bearing should be less prone to thermal seizure effects compared to the cylindrical bearing. The present results show that stable or unstable Morton effects can be triggered by different unbalances when the rotor is operated close to its first flexible mode.

2 Test rig description

The test rig illustrated in **Figure 3** is composed of a hollow shaft driven by a 1.8 kW DC Motor and a flexible coupling. The maximum attainable speed is 10 krpm. The rotor is guided by a ball bearing at is drive end (DE) and by a Flexure Pivot Tilting Pad Journal Bearing (FPTPJB) at its non-drive end (NDE). The total length of the rotor is 790 mm. The inner and outer diameters of the shaft are 35 mm and 45 mm, respectively. The distance between the bearing centrelines is 520 mm.

Four disks are mounted on the rotor: two heavy disks (Disk 2 of 6.4 kg mounted between the bearings and Disk 4 of 10.4 kg overhung mounted) and two small disks (Disk1 and 3) installed between the central disk and the bearings. The inertia characteristics of the small disks are negligible compared to the heavy disks but they serve as additional balancing planes. The static loads of the FPTPJB and of the ball bearing are 175 N and 30 N, respectively.

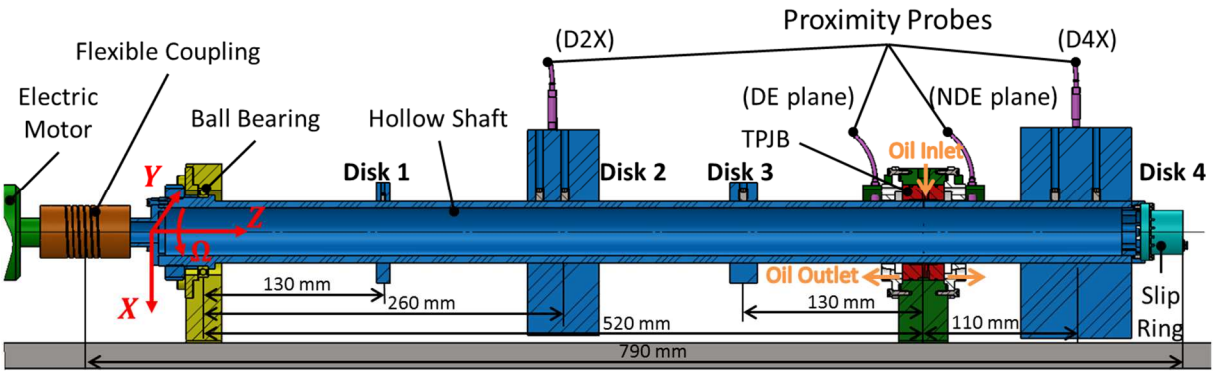

Figure 3. Description of the test rig

2.1 The design of the flexure pivot tilting pad bearing

The FPTPJB shown on the **Figure 4** and described in **Table *2*** was made of one piece of bronze. The pads were cut by wire electrical discharge machining and the pivots are flexible micro-beams. The bearing has the advantages of the classical tilting pad bearing without the complexity of multi-piece design, i.e. no wear between the pad and the pivot and no stack-up tolerances. The bearing has four pads, P1-P4 and four feeding pockets, Fp1-Fp4 located between pads. The lubricant is ISO VG 32 turbine oil (the kinematic viscosity is 25.1 cP @ 40°C and 11.5 cP @ 60°C) supply at ambient room temperature. The feeding temperature was not controlled. However, the large volume of lubricant in tank secured a quasi-constant feeding temperature.

Table 2. Geometrical characteristics of the FPTPJB

Rotor diameter	45 mm	Pad number	4
Pad axial length	30 mm	Pad arc length	72°
L/D ratio	0.67	Pivot offset	60 %
Radial bearing clearance	50 µm	Pivot length	2.5 mm
Radial pad clearance	75 µm	Pivot width	0.75 mm
Pad preload	0.33	Static load	LBP

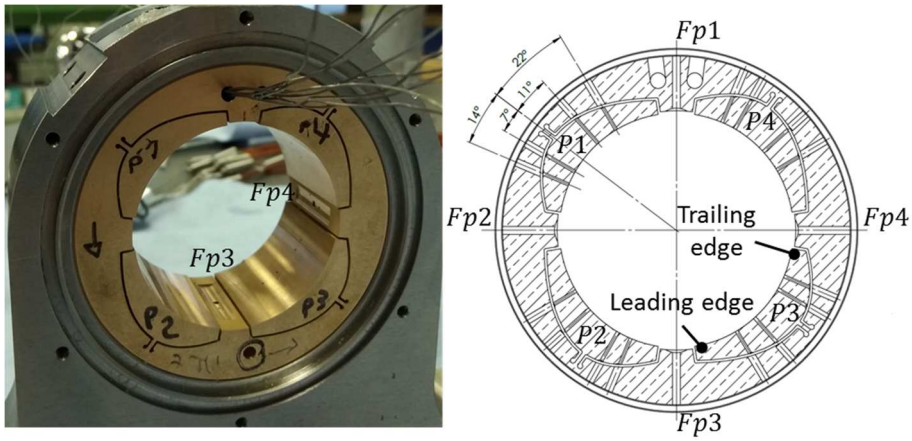

Figure 4. Geometry of the FPTPJB

2.2 Instrumentation

The test rig is instrumented with six inductive proximity probes, two orthogonally mounted at each side of the FPTPJB (DE plane, NDE plane on **Figure 3**), and two mounted on the disks in the X direction (D2X and D4X on **Figure 3**). The temperatures at the bearing surface are measured on each pad by four thermocouples mounted in its mid plane. Their circumferential position is shown on **Figure 4**. Four other thermocouples measure the temperature in the feeding pockets and another thermocouple measures the oil inlet temperature. The rotor is also equipped with five thermocouples in the journal mid plane, equally spaced circumferentially and connected to a slip ring shown on **Figure *3***. All thermocouples are of T type with 0.5°C accuracy. In order to limit the influence of the thermocouples on the journal bearing flow, their diameter was 0.5 mm and they were all flush mounted on the pads and on the rotor surface. The supply pressure and flow rate are also measured at the bearing inlet.

2.3 Linear dynamic analysis of the rotor-bearing system

The Campbell and the stability diagrams of the rotor-bearings system are presented on **Figure 5**. They are computed by using theoretical rotordynamic coefficients for the FPTPJB [27] and a constant direct stiffness of $3 \cdot 10^8$ N/m for the ball bearing.

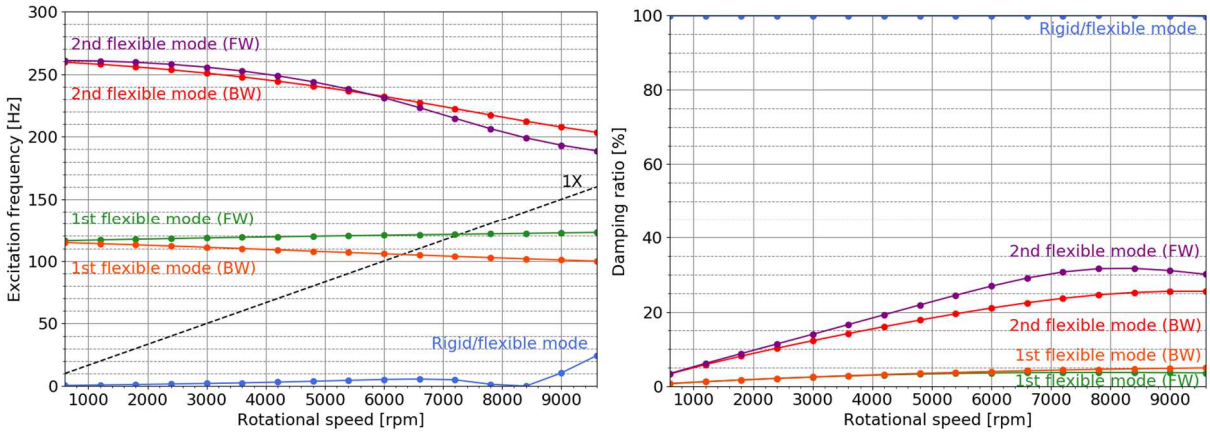

Figure 5. Campbell and stability diagrams

A first rigid mode is present at very low frequencies and is highly damped. The first flexible modes are located at 6.3 krpm (backward) and at 7.3 krpm (forward). The forward mode has a damping ratio less than 5%. This small value of the damping ratio indicates that the rotor will generate high amplitude vibrations close to 7.3 krpm and it is very likely that this speed cannot be crossed. The shape of the first flexible forward mode is depicted in **Figure 6**.

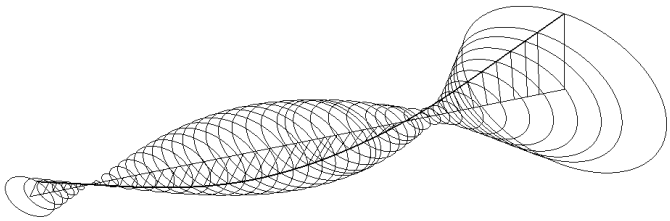

Figure 6. The shape of the first flexible forward mode

3 Experimental results

A two-plane balancing of the rotor (using disk 2 and disk 4) at 4 krpm was performed. Balancing at higher speeds, close to the frequency of the 1st flexible mode proved to be difficult. Therefore, all the tests were performed at rotational speeds below the frequency of the 1st flexible forward mode.

As explained in the introduction, the rotor may exhibit unstable synchronous vibrations depending on the position of the thermal unbalance relative to the hot spot. Since the rotor will operate below the critical speed, the vibration vector may become unstable if the thermal imbalance is in phase with the hot spot (Case 1 of **Table 1**). In this case, the rotation of the vibration vector is opposite to the rotational

speed. On the other hand, if the thermal imbalance is out of phase with the hot spot, the vibration vector tends towards an equilibrium position.

This explanation is rigorous for the Newkirk effect and the Morton effect is similar. The main difference between the Newkirk and the Morton effect comes from the position of the hot spot. For the Newkirk effect, the hot spot is very close to the contact point which itself is the high spot. For the Morton effect, the hot spot is located behind the high spot because the heat is generated by shearing the thin lubricant fluid film.

To trigger the Morton effect, the amplitudes of the synchronous vibrations must be large enough to generate heat in the fluid film. Therefore, the tests will be performed at rotational speeds close to the first bending mode with different unbalances on the disk 2 and / or on the disk 4.

3.1 Test 1. Stable synchronous vibrations

The first test was conducted with an unbalance of 230 g·mm@-110° on the disk 2 and 160 g·mm@60° on the disk 4. The inlet temperature, the pressure and the flow rate are 22°C, 0.1 bar and 0.1 l/min, respectively. The speed was increased up to 6.55 krpm in 200 s and was kept constant for 90 s.

Figure 7 presents the amplitude and the phase of synchronous vibrations obtained from FFT of NDEY proximity probe data for the complete test including start-up and coast-down. During start-up, the amplitude is very low (<4 µm) up to 5.6 krpm, then increases rapidly up to 6.55 krpm. The speed was then kept constant for 90 s. At this constant speed, the NDEY amplitude increases again from 30 µm to 55 µm. During deceleration, the amplitude is larger than during the start-up phase down to 4.2…4.6 krpm. The same behaviour is observed for the synchronous phase depicted in **Figure 7**b. This clear hysteresis shows that a thermal effect is present during the test, particularly at constant speed.[1]

[1] Thermal effects have a time scale of the order of seconds, much larger than the 10^{-3} s time scale of rotordynamic effects. Their signature is therefore a typical hysteresis.

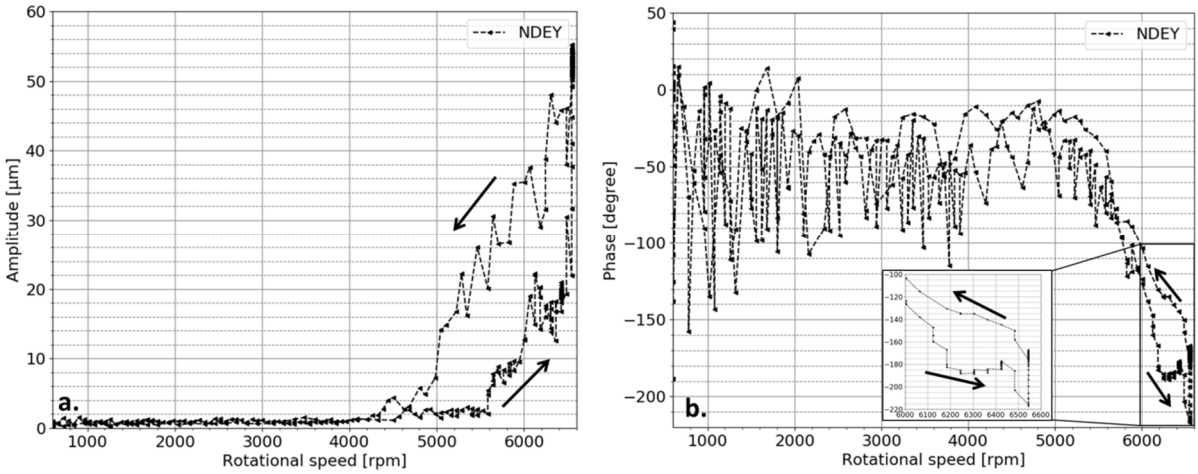

Figure 7. Synchronous vibration at NDEY recorded during start-up and coast-down of test 1. a. Amplitudes. b. Phases.

Figure *8* presents the time variation of the synchronous amplitudes and phases at the constant speed of 6.55 krpm (i.e. starting with 200 s). From 200 s to 210 s, the amplitudes and the phases vary rapidly. After 210 s, they vary slowly before becoming constant starting with 240 s.

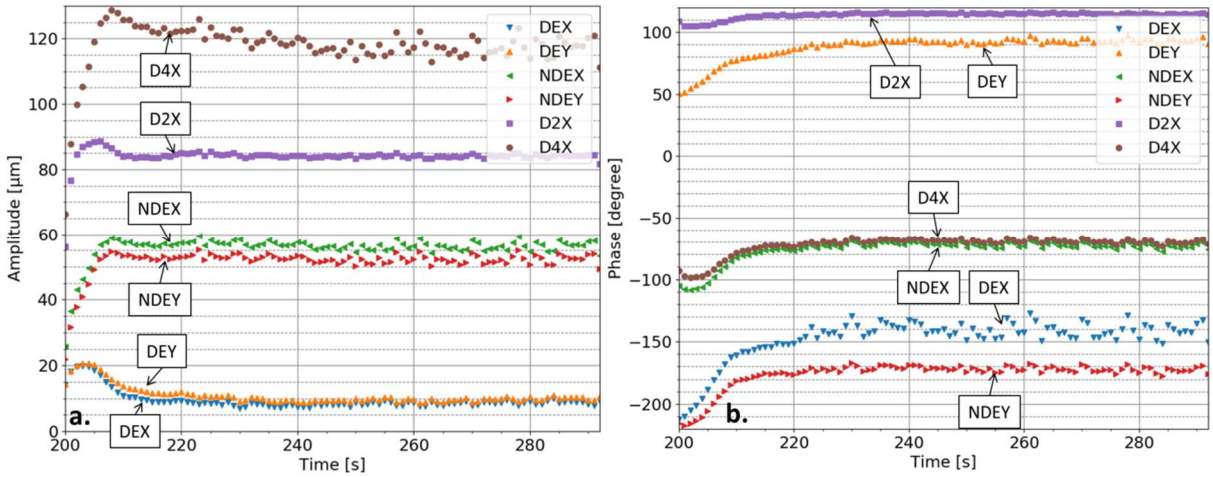

Figure 8. Synchronous response at 6.55 krpm for test 1. a. Amplitudes. b. Phases.

A polar plot of the amplitudes and the phases measured at constant speed is depicted in **Figure *9***. The amplitudes increase is largest in planes D2 and D4 located far from the bearing and corresponding to the two disks. The phases indicate a counter-clockwise rotation, i.e. the vibration vector rotates in the same (forward) direction as the rotational speed.

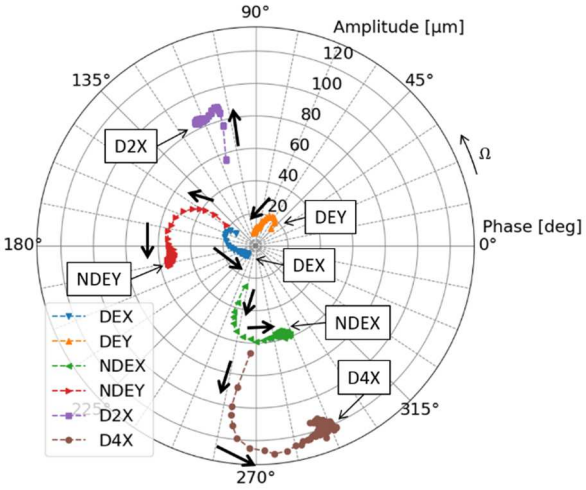

Figure 9. Polar plot of the synchronous response at 6.55 krpm for test 1.

The stable, forward spiralling vibration vectors depicted in Figure 9 can be explained as it follows. ***Figure 8***a shows that the disk D4 has by far the largest synchronous amplitude. The phases of disks D2 and D4 after 220 s are 115° and -70°, respectively (***Figure 8***b). This indicates a conical vibration of the rotor near the journal bearing, with a large amplitude of the overhung mass clearly distinguishable in **Figure *9***. The large difference between the DE and the NDE amplitudes (***Figure 8***a) comfort this remark. This is the situation depicted in ***Figure 1***b, when the thermally induced unbalance is on the overhung disk and out of phase with hot spot (HS). The upper right corner of ***Table 1*** and of ***Figure 2*** indicate that for this case the Morton effect is stable and the spiral is forward (i.e. in the direction of the rotational speed).

The journal temperature in the bearing mid-plane recorded by the 5 equally spaced thermocouples is depicted in **Figure *10***a. A cubic polynomial interpolation was used to determine the maximum and minimum temperatures that are superimposed on **Figure *10***a.

Following the isolines depicted in **Figure *10***a., at the beginning of the test (from 200s to 210s), the hot spot has not a clear location; it could be circumferentially located close to 100° or close to 270° relative to the keyphasor (i.e. the zero-phase reference point in the journal reference frame). After 210 s, the location of the hot spot is unambiguous and close to 100° relative to the keyphasor. A blue line indicates the cold spot in **Figure *10***a. The maximum journal temperature difference, $\Delta T = T_{max} - T_{min} = Red\ line - Blue\ line$ is depicted in **Figure *10***b. The temperature difference increases quickly from 5.5°C at 200 s to 9.5°C at 210 s, and then decreases slowly.

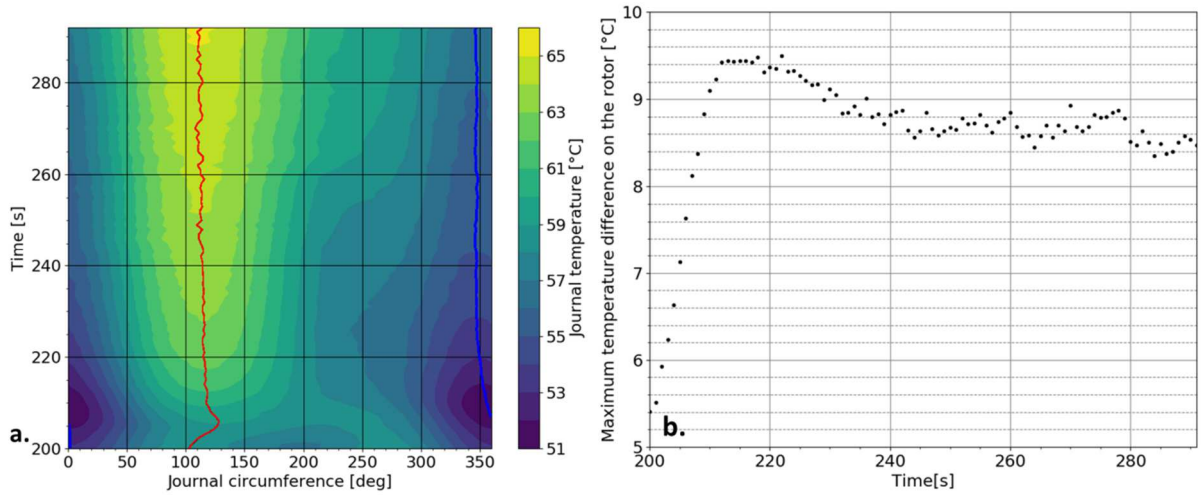

Figure 10. Time variation of the journal temperature in the bearing mid-plane for test 1; a-Surface plot (red and blue lines indicate the hot and cold spots, respectively); b-Maximum journal temperature difference ΔT measured in bearing mid-plane vs. time.

Examples of synchronous orbits in the DE and NDE planes recorded every second are depicted in **Figure *11***. As mentioned, the test rig is equipped with two pairs of proximity probes solidly mounted at the DE and the NDE ends of the journal bearing. The clearance limits of the journal bearing are obtained by gently pushing the rotor against the bearing pads at zero speed. This is the almost square profile depicted in ***Figure 11*** and its center is the center of the journal bearing. Dynamic displacements are measured by the same proximity probes during operating conditions and yield the orbits that are plotted in ***Figure 11***. The position of the high spot is extracted from these orbits. It is therefore considered that the time variations of the orbit are slow and the rotor center describes a synchronous orbit at each moment. For each orbit, the vector between the center of the bearing and the center of the rotor describing this orbit defines the high spot. This vector appears as whirling in a fixed reference frame.

In a reference frame rotating with the journal, the circumferential position of the high spot relative to the zero-phase reference (the keyphasor) is constant only if the orbit is centered and circular. As shown in **Figure *11***, the synchronous orbits are eccentric ellipses, the trend being stronger for orbits in the DE plane. This leads to a continuous variation of the phase difference between the high spot and the zero-phase reference. Therefore, this phase is described by two parameters: an orbit averaged value and a standard deviation indicating the error that is made by considering a constant value of the phase of the high spot. This process is completely detailed in [26].

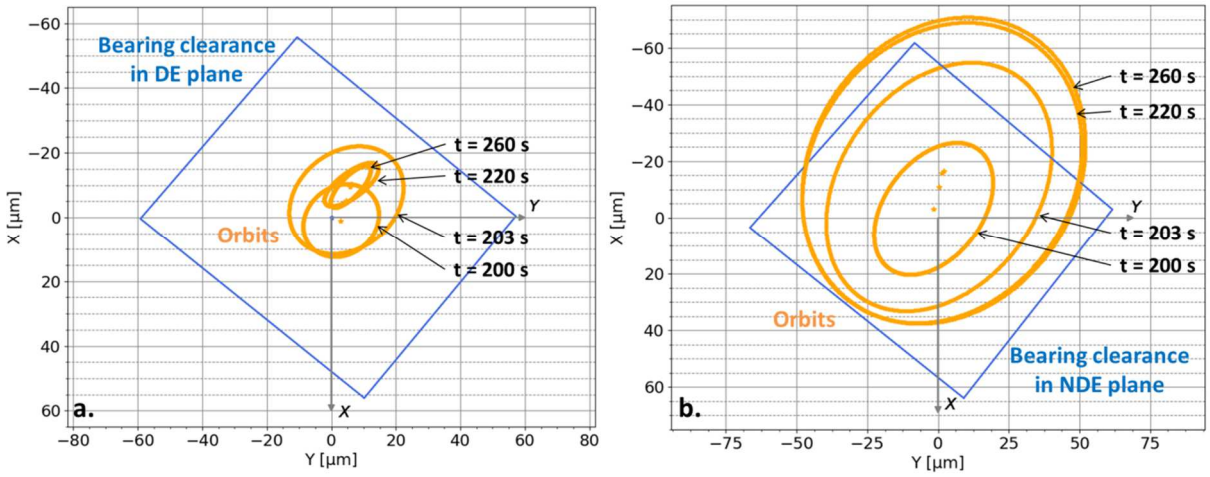

Figure 11. Synchronous orbits measured for test 1. a. DE plane, b. NDE plane.

The average values of the phase lag between hot spot and the high spot are plotted in **Figure *12***. The phase error bars represent the standard deviation resulting from the high spot describing eccentric and/or elliptic orbits. The standard deviation is very large in the DE plane because the orbits in this plane are eccentric. For example, the orbits at 203 s and at 220 s depicted in **Figure *11***a are both elliptical. However, the orbit at 203 s is almost centred and the standard deviation is small (≈10°), while the orbit at 220 s is eccentric and the calculated standard deviation is so large that it cannot be considered as meaningful. It is therefore not possible to interpret the phase lag between the hot spot and the high spot in the DE plane.

The phase lag between the hot spot and high spot in the NDE plane has a small standard deviation. It is negative at the beginning of the time interval (the high spot lags the hot spot), increases quickly to a phase lag of 40° and then decreases slowly to 30-35°. This value is in agreement with the literature [24].

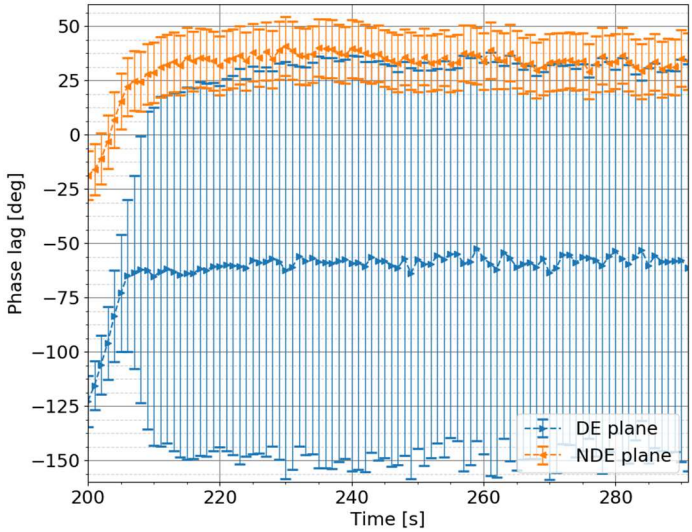

Figure 12. Phase lag between hot spot and high spot in the DE and NDE planes for the test 1.

A second piece of information that can be extracted from the rotor orbits is the trajectory of the orbit center at the DE and NDE planes during run-up and at constant speed. These trajectories are depicted in ***Figure 13***. The distance between the rotor orbit center in DE plane and the NDE plane indicate a misalignement of the journal bearing that remains almost unchanged during run-up and at constant speed. This enforces the previous remark of a conical vibration of the rotor near the journal bearing.

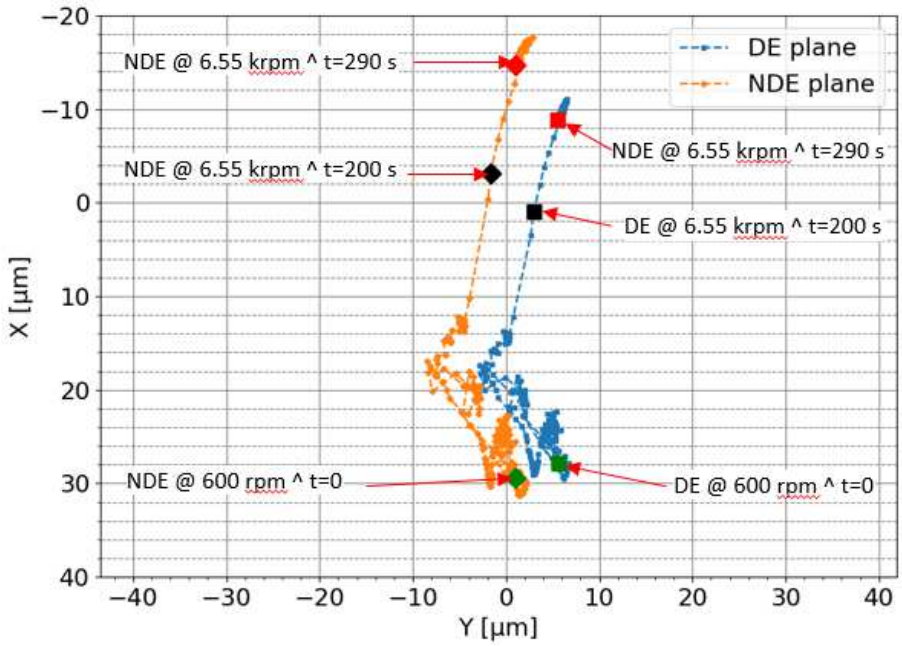

Figure 13. Trajectories of the rotor orbit center at DE and NDE planes during run-up and at constant rotational speed (6.55 krpm) for the test 1.

The time variations of the pad average temperature and of the pad maximum temperature difference for each pad are depicted in **Figure *14***. The pad P3 that supports the largest part of the rotor weight has also the largest thermal loading. The pads P1 and P4 that do not support the rotor weight have a smaller thermal loading. However, their temperature rise is not negligible because the journal describes large synchronous amplitudes due to the large dynamic load.

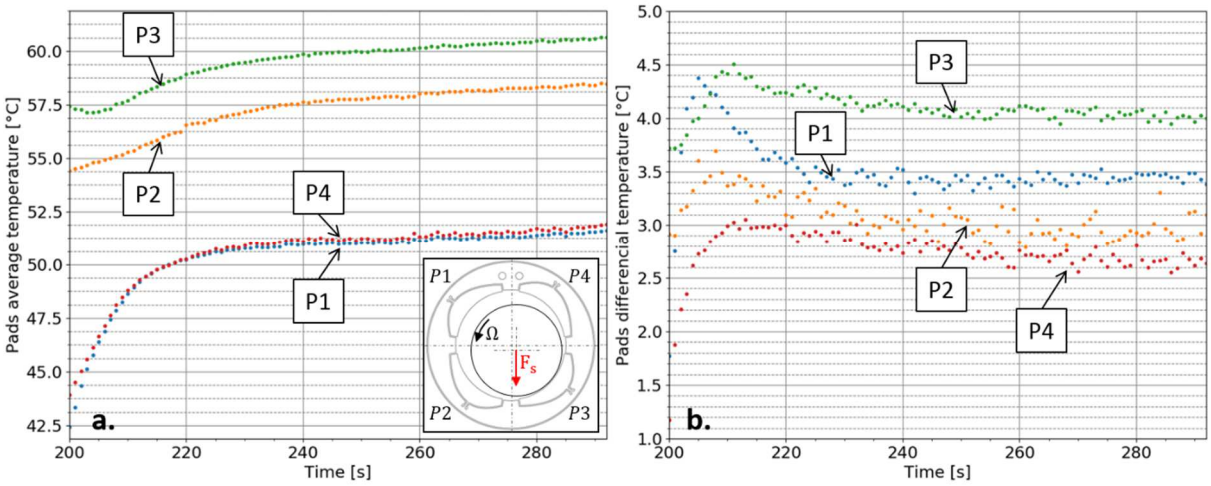

Figure 14. Time variation of the pad average temperature (a) and of the pad maximum temperature difference (b) for test 1

The test 1 was repeated 10 times for estimating the measurement accuracy and repeatability. The results (synchronous amplitudes and phases, journal temperatures) are presented in the **Appendix**: Repeatability of the tests results. The errors are close to 5 µm for the synchronous amplitudes, negligible for the synchronous phases and lower that 0.5° for the temperatures.

3.2 Test 2. Unstable synchronous vibrations

The second test was conducted with an unbalance of 220 g·mm @ 6° on disk 2 and 160 g·mm @ 60° on disk 4. The inlet temperature, pressure and flow rate are 23°C, 0.1 bar and 0.1 l/min, respectively. The first difference between test 1 and test 2 is the angular position of the unbalance on disk 2 (for test 1 the additional unbalance is 230 g·mm @ -110°). The second difference is that the speed was increased to 6.85 krpm in 530 s and was kept constant for 100 s.

Figure *15* presents the synchronous vibrations vector NDEY versus rotor speed for the whole test. As for the test 1 (**Figure *7***), the synchronous amplitude and phase show a hysteresis.

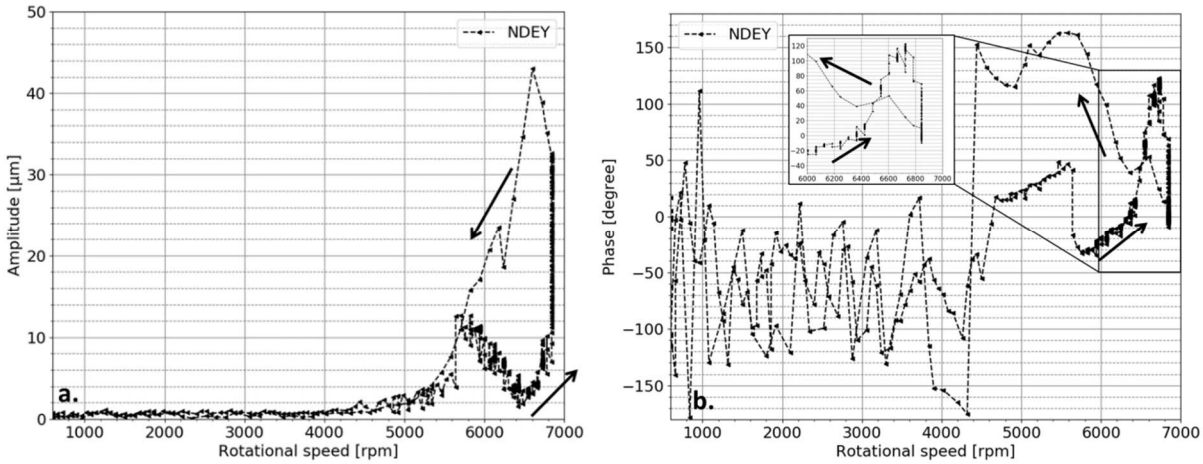

Figure 15. Synchronous vibrations NDEY recorded during start-up and coast-down in test 2. a. Amplitudes. b. Phases.

The amplitudes and phases of the synchronous vibrations at constant speed (6.85 krpm) are plotted on **Figure *16***. At the beginning of the constant speed time interval, the amplitudes D2X and D4X increase to a maximum then decrease (**Figure *16***a.). However, at the middle of the test, the amplitude D4X increases again. The amplitudes in the NDE plane increase constantly during the entire time interval while in the DE plane they increase up to 600 s then they decrease slightly. Therefore, at the end of the test, all NDE sensors (NDEX, NDEY, D4X) show an increasing tendency while all DE sensors show a decreasing tendency. This shows that the rotor is bent very close to the bearing.

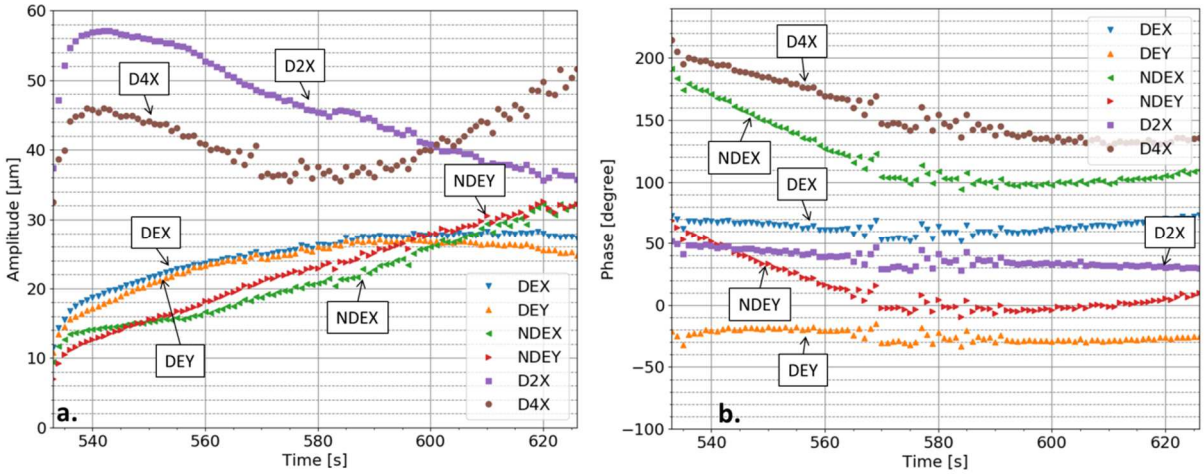

Figure 16. Synchronous vibrations at 6.85 krpm for test 2. a. Amplitudes. b. Phases.

Polar plots of the synchronous vibration vectors are depicted in **Figure *17***. They show that the amplitudes of the vibration vectors increase (more rapidly at the beginning of the time interval) and they rotate in the opposite (backward) direction to the rotational speed. The trend changes in the last part of the time interval with amplitudes NDEX, NDEY and D4X showing a pronounced increase. The test was therefore stopped to avoid any journal bearing damage.

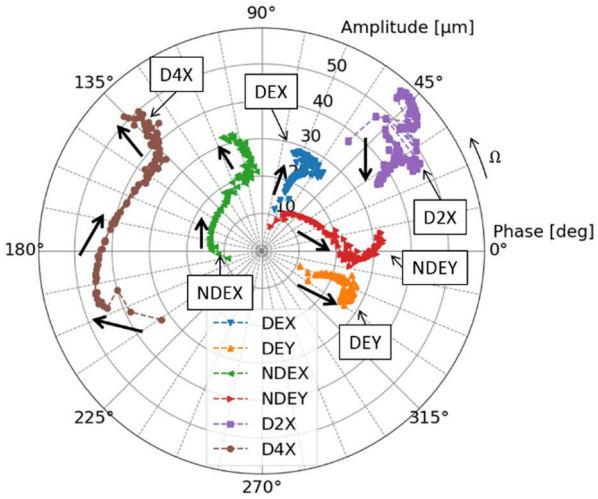

Figure 17. Polar plot of the synchronous response at 6.85 krpm for test 2.

The backward spiralling vibration vectors depicted in Figure 16 are explained as for Test 1. ***Figure 16***a shows that at 580 s the synchronous amplitudes of disks D2 and D4 are 46 µm and 38 µm, respectively. The values are quite close but with a larger amplitude of D2. The situation is similar for the amplitudes measured in the DE and NDE planes. At the same moment, the phases of disks D2 and D4 are 40° and 150°, respectively (***Figure 16***b). This indicates a mixed cylindrical-conical vibration with a larger amplitude of disk D2. This situation is close to the one depicted in ***Figure 1***a, when the thermally induced unbalance is on the middle disk and in phase with hot spot (HS). The upper left corner of ***Table 1*** and of ***Figure 2*** indicate that for this case, the Morton effect is unstable and the spiral is backward (i.e. opposite to the rotational speed). This situation prevails as long as the synchronous amplitude of D2 is larger than the amplitude of D4 (or the amplitudes at the DE plane are larger than the amplitudes at the NDE plane). After this moment, the vibration vectors do not follow a spiral anymore and start increasing rapidly. It seems that the thermal unbalance shifts from the middle disk D2 to the overhung disk D4.

The time variation of the journal temperature in the bearing mid-plane is depicted in **Figure *18***. The isolines of the circumferential temperatures of the rotor versus time (**Figure *18***a) are to be compared

with the results obtained for test 1 and depicted in **Figure *10***a. Both figures show clear values of the maximum and minimum temperatures (marked with red and blue lines, respectively) but the maximum temperatures in **Figure *18***a. are located at 250° relative to the zero-phase reference. Moreover, in **Figure *18***a. there is no ambiguity on the location of the hot spot at the first moments of test 2. This was not the case for test 1 (**Figure *10***a). **Figure *18***b. depicts the maximum journal temperature difference measured in the bearing mid-plane. The temperature difference shows a constant increase during test 2. This was not the case of the test 1 (**Figure *10***b) were the temperature difference increased rapidly in the first moments then decreased asymptotically.

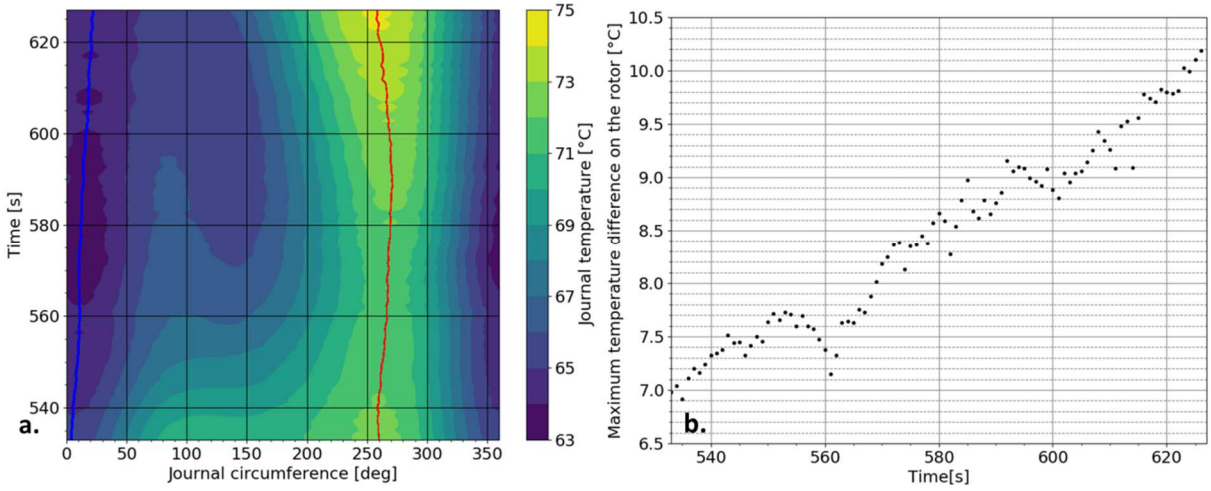

Figure 18. Time variation of the journal temperature in the bearing mid-plane for test 2; a-Surface plot (red and blue lines indicate the hot and cold spots, respectively); b-Maximum journal temperature difference ΔT measured in bearing mid-plane vs. time.

Some of the synchronous orbits used for extracting the position the high spot in test 2 are depicted in **Figure *19*** for the DE and NDE planes. The orbits have large amplitudes and are less eccentric than those depicted in **Figure *11***a. for test 1. The extraction of the angular position of the high spot is therefore more accurate. **Figure *20*** depicts the phase lag between the hot spot and the high spot for test 2. Compared to **Figure *12*** obtained for test 1, the phase lags depicted in **Figure *20*** show much lower standard deviations and can therefore be interpreted. They show that in the NDE plane the hot spot is located before the high spot but the phase lag decreases from 50° (a common value of the phase difference) to almost 0° indicating that at the end of the time interval the hot and the high spots are very close. The small value of the phase lag between hot and high spots is characteristic for the Newkirk effect, i.e. for operating conditions very close to contact between the synchronously whirling journal and

the bearing [26]. The situation is different in the DE plane where the phase lag between the hot and the high spot is negative, i.e. the hot spot precedes the high spot. Such of a situation may occur only when the rotor is bent between the DE and the NDE planes. In this case the journal bearing will be also misaligned not only eccentric.

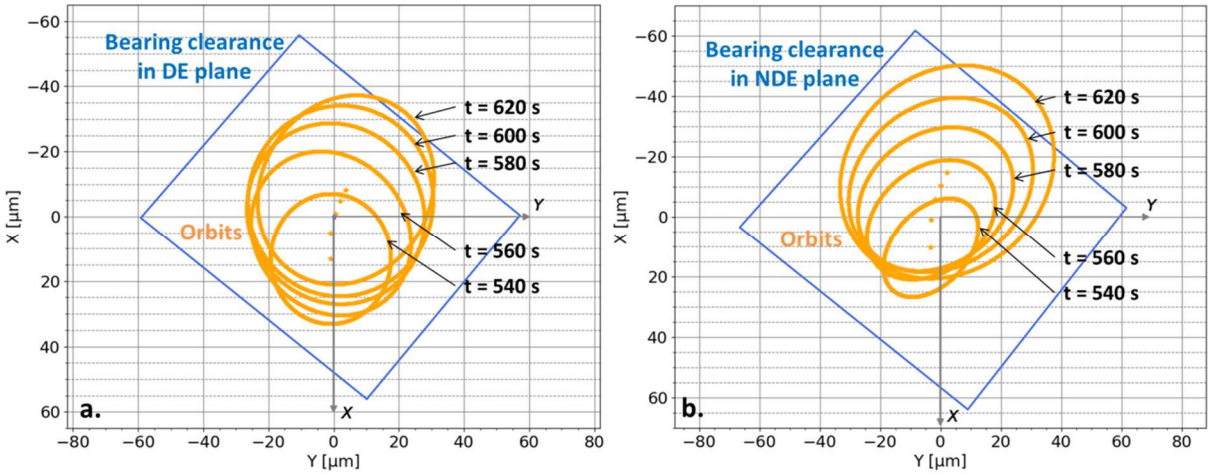

Figure 19 Synchronous orbits measured for test 2. a. DE plane, b. NDE plane.

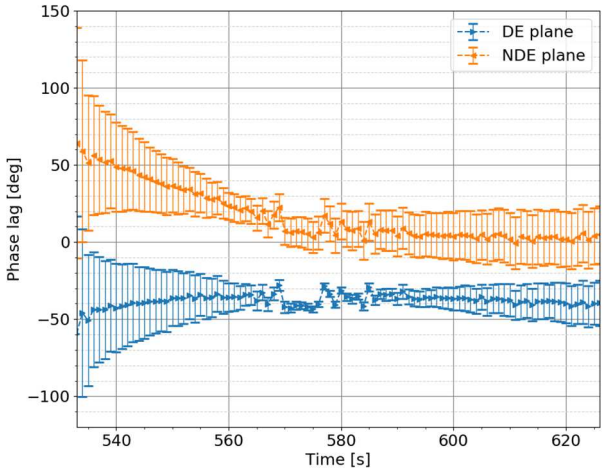

Figure 20 Phase lag between hot spot and high spot in the DE and NDE planes for the test 2.

The trajectories of the orbit center at the DE and NDE planes during run-up and at constant speed are depicted in ***Figure 21***. At the 600 rpm, the centers of the orbits depicted in ***Figure 13*** (for test 1) and ***Figure 21*** (for test2) coincide in the DE plane and NDE plane, respectively. However, ***Figure 21*** shows that during run-up and at constant rotational speed, the distance between the centers of the orbits in the DE and the NDE plane in test 2 are less important than in test 1. This indicates that the journal bearing

is less misaligned in test 2 than in test 1, remark that was also made when discussing the backward spiralling vibrations of test 2.

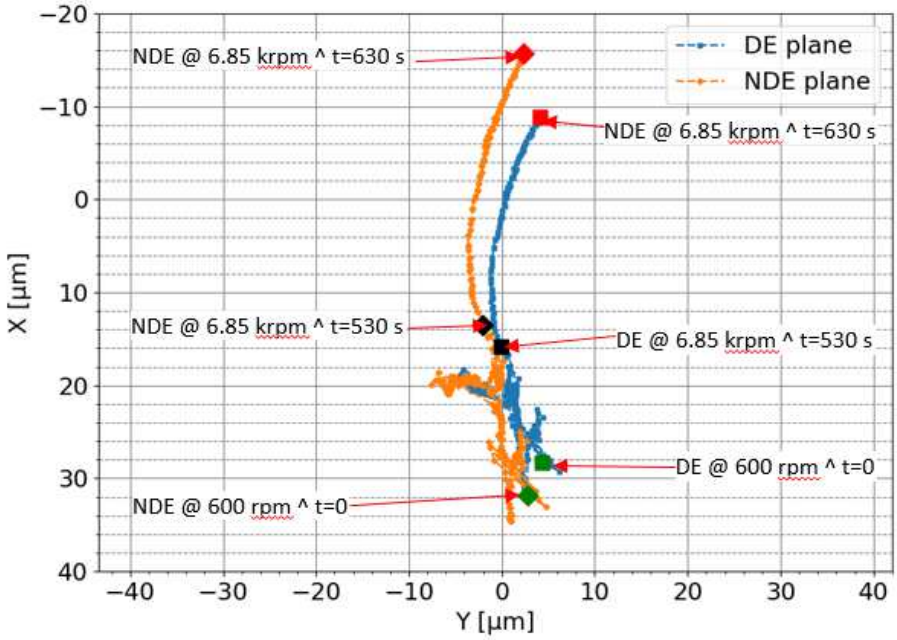

Figure 21. Trajectories of the rotor orbit center at DE and NDE planes during run-up and at constant rotational speed (6.85 krpm) for the test 2.

The time variations of the pads average temperatures and maximum temperature differences are depicted in **Figure *22***. As for test 1, the pads P2 and P3 have the largest thermal loading. However, the average temperatures increase more rapidly in time and the maximum temperature differences have different trends compared to test 1. This indicates a different dynamic regime of test 2 compared to test 1.

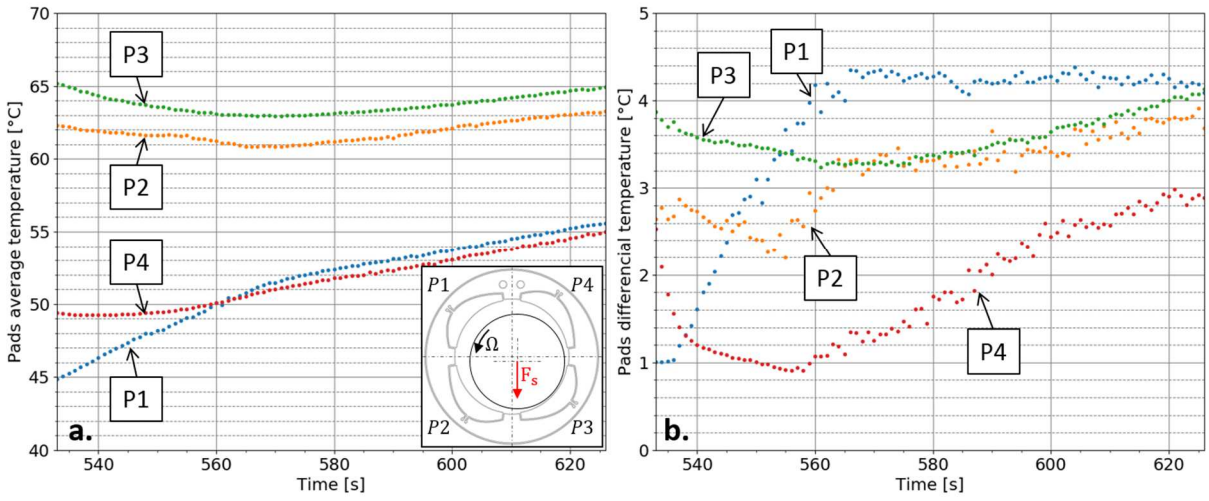

Figure 22 Time variation of the pad average temperature (a) and of the pad maximum temperature difference (b) for test 2

4 Conclusions

The experimental results obtained for a flexible rotor supported by a ball bearing and a flexure pivot tilting pad bearing confirm the possibility of triggering thermally induced, synchronous vibrations. The synchronous amplitudes and phases measured at the DE and NDE planes as well as on disks D2 and D4 corroborated with the theoretical elements obtained from simple models explain the measured forward or backward spiralling vibration vectors.

The typical spiral form of these vibrations is much clearer in the present measurements than in the previous tests obtained with the same test rig and rotor and presented in [26]. The main difference between the two test campaigns was the journal bearing. A cylindrical journal bearing was used for the first test campaign presented in [26] while a flexure pivot tilting pad bearing was used in the present one. The results of the first test campaign suggested that large amplitude synchronous vibrations triggered also a bearing seizure and that the effect of reducing the radial clearance of the cylindrical bearing gradually became dominant. This can be explained by the fact that the cylindrical bearing could accommodate thermal deformations only by reducing its diameter. The situation is different for the presently used flexure pivot tilting pad bearing. The presence of pads and the flexible pivot enable the accommodation of thermal deformations with less impact on the radial clearance. The risk of seizure is therefore reduced and the rotor describes spiral synchronous vibrations. However, these vibrations can lead to either stable or unstable operating regimes depending on the magnitude and distribution of the mechanical unbalance.

Not the least, the paper contains all the details of the test bench and the information from the measurements to serve as a database for comparisons with theoretical models of the Morton effect.

5 References

[1] B.L. Newkirk, Shaft Rubbing, Mechanical Engineering 48 (1926) 830–832.

[2] A.D. Dimarogonas, Newkirk Effect: Thermally Induced Dynamic Instability of High- Speed Rotors, Gas Turbine Conf. Prod. Shows, Washington, D.C., ASME Paper No. 73-GT-26 (1973).

[3] A.D. Dimarogonas, A Study of the Newkirk Effect in Turbomachinery, Wear 28, (1974) 369–382.

[4] W. Kellenberger, Spiral Vibrations Due to the Seal Rings in Turbogenerators Thermally Induced Interaction Between Rotor and Stator, J. Mech. Des. 102(1) (1980) 177-184.

[5] O. Matsuhita, M. Tanaka, H. Kanki, M. Kobayashi, P. Keogh, Vibrations of Rotating Machinery Vol1. Basic Rotordynamics: Introduction to Practical Vibration Analysis, Springer Japan (2017).

[6] P.G. Morton, Some Aspects of Thermal Instability in Generators, G.E.C. Internal Report No. S/W40 u183 (1975).

[7] B. Hesseborn, Measurements of Temperature Unsymmetries in Bearing Journal Due to Vibration, Internal report ABB Stal. (1978).

[8] L. Gu, A Review of Morton Effect: From Theory to Industrial Practice, Tribol. Trans. 61(2), (2017) 381–391.

[9] X. Tong, A. Palazzolo, J. Suh, A Review of the Rotordynamic Thermally Induced Synchronous Instability (Morton) Effect, Appl. Mech. Rev. 69 (2017).

[10] F.M. de Jongh, The Synchronous Rotor Instability Phenomenon - Morton Effect, 47th Turbomach. & 34th Pump Symp (2018).

[11] N. Takahashi, M. Hiroshima, H. Miura, Y. Fukushima, Dynamic Instability Induced by Iron Loss Unbalance in Rotor-Active Magnetic Bearing System, Trans. Japan Soc. Mech. Eng. Ser. C 69(685), (2003) 2287–2294.

[12] N. Takahashi, S. Kaneko, Thermal instability in a magnetically levitated doubly overhung rotor, J Sound Vib 332(5), (2013) 1183–1203.

[13] F.M. de Jongh, P.G. Morton, The Synchronous Instability of a Compressor Rotor Due to Bearing Journal Differential Heating, J. Eng. Gas Turbines Power, 118(4), (1996) 817–823.

[14] F.M. de Jongh, P. van der Hoeven, Application of a Heat Barrier Sleeve, Proc. 27th Turbomach. Symp., Texas A&M University, College Station, TX, (1998) 17–26.

[15] F. Berot, H. Dourlens, On Instability of Overhung Centrifugal Compressors, Proc. Gas Turbine Aeroengine Congr. Exhib., Indianapolis, Indiana, June 7-10, ASME paper No. 99-GT-202 (1999).

[16] J.A. Kocur, F.M. de Jongh, Thermal Rotor Instability in Gas Compressors, AVPG 14th International Gas Convention (2000).

[17] W. Marscher, B. Illis, Journal Bearing " Morton Effect " Cause of Cyclic Vibration Compressors, Tribology Transactions 50.1 (2007), 104–113.

[18] J. Schmied, J. Pozivil, J. Walch, Hot Spots in Turboexpander Bearings : Case History, Stability, Analysis, Measurements and Operational Experience, Proc. ASME Turbo Expo 2008 : Power land, sea and air, June 9-13, Berlin, Ger., GT2008-51179 (2008).

[19] J.A. Lorenz, B.T. Murphy, Case Study of Morton Effect Shaft Differential Heating in Variable Speed Rotating Electric Machine, Proc. ASME Turbo Expo 2011, GT2011-45228 (2011).

[20] A.C. Balbahadur, A Thermoelastohydrodynamic Model of the Morton Effect Operating in Overhung Rotors Supported by Plain or Tilting Pad Journal Bearings, Doct. Dissert., Virginia Polytechnic Institute and State University (2001).

[21] P.J. Bradley, Fundamental Study into the Governing Conditions of Rotor Thermal Bows in Hydrodynamic Bearings, Doct. Dissert. Cranfield University (2012).

[22] D. Panara, L. Baldassare, S. Panconi, E. Meli, D. Griffini, A. Mattana, Numerical Prediction and Experimental Validation of Rotor Thermal Instability, 44th Turbomach. & 31st Pump Symp. (2015).

[23] B.T. Murphy, J.A. Lorenz Simplified Morton Effect Analysis for Synchronous Spiral Instability, J. Vib. Acoust. 132.5 (2010) 1–7.

[24] X. Tong, A. Palazzolo, Measurement and Prediction of the Journal Circumferential Temperature Distribution for the Rotordynamic Morton Effect, J. Tribol. 140.3 (2018) 1–25.

[25] A. Hresko, D. Shin, A. Palazzolo, Experimental Investigation of Morton Effect (Thermally Induced Rotor Instability), Proc. ASME Turbo Expo 2019 Turbomach. Tech. Conf. Expo. June 17-21, Phoenix, USA, ASME Paper GT2019-92281 (2019).

[26] T. Plantegenet, M. Arghir, M.A. Hassini, P. Jolly, The Thermal Unbalance Effect Induced by a Journal Bearing in Rigid and Flexible Rotors: Experimental Analysis, Tribology Transactions 63.1 (2020), 52–67. DOI: 10.1080/10402004.2019.1658836.

[27] T. Plantegenet, Analyse expérimentale de l'effet Morton (in French), Doct. Dissert. Université de Poitiers, France (2019).

Appendix: Repeatability of the tests results

The test 1 was performed ten times in order to show the repeatability of the results. The ten tests have the same operating conditions (starting speed, unbalance, inlet temperature, inlet pressure, inlet flow rate). ***Figure 23*** shows the synchronous amplitudes and phases for test 1 with average values and error bars representative for the standard deviation. For the synchronous amplitudes (***Figure 23***a.) the

standard deviation is less than 5 µm in the DE and NDE planes near the bearing. On the disks D2 and D4, the standard deviation is also close to 5 µm with maximum values of 10 µm. For the synchronous phases, the standard deviation is low for all measurements.

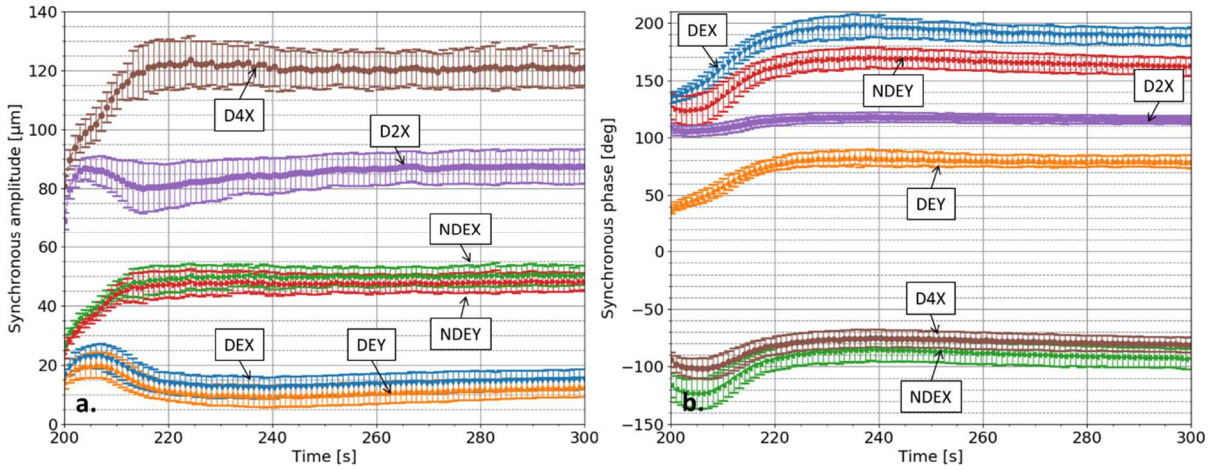

Figure 23. Synchronous amplitudes (a.) and phases (b.) for the test 1 repeated ten times

The average temperature of the journal is plotted in **Figure *24***a. The error of the average temperature is close to 3°C. This is explained by the global temperature of the test rig. For example, the temperature of the bearing housing is close 25°C at the beginning of the first test, but for the second one, the temperature becomes close to 30°C. However, this error does not affect the variation of the average temperature. **Figure *24***b. shows the journal temperature differences for the ten tests. They show a good repeatability with an error lower than 0.5°C (i.e. the accuracy of the thermocouple).

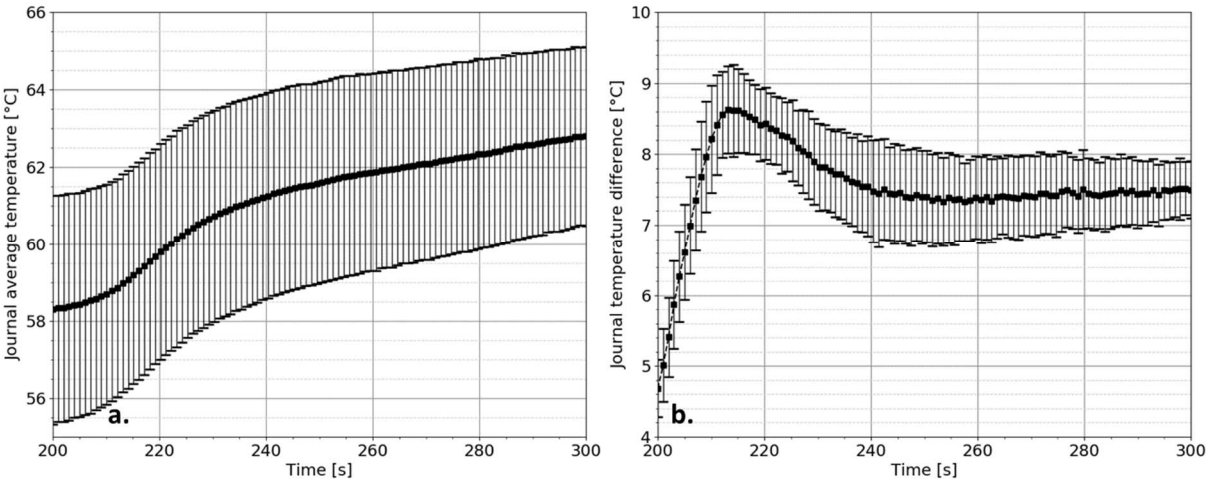

Figure 24. Journal average temperature (a.) and journal temperature difference (b.) for the test 1 repeated ten times